

Scattering of diffuse photon density waves by spherical inhomogeneities within turbid media: Analytic solution and applications

D. A. BOAS^{†‡}, M. A. O'LEARY^{†‡}, B. CHANCE[‡], AND A. G. YODH[†]

Departments of [†]Physics and [‡]Biochemistry and Biophysics, University of Pennsylvania, Philadelphia, PA 19104

Contributed by B. Chance, December 30, 1993

ABSTRACT We present an analytic solution for the scattering of diffuse photon density waves by spherical inhomogeneities within turbid media. The analytic result is compared to experimental measurements. Close agreement between theory and experiment permits the use of the theory to determine the properties of unknown sphere-like objects embedded in turbid media. The analytic solution is extended to encompass several problems of practical interest in imaging, including the influence of multiple sources, multiple objects, and boundaries on the characterization of spherical inhomogeneities. We also extend the solution to encompass time-domain measurements.

Recently, useful information about turbid media such as human tissue has been derived from photons migrating through these media (1). The diffusing photons enable us to noninvasively probe highly scattering materials and determine their average scattering and absorption properties (2, 3). Furthermore, the diffusing photons can also be utilized in imaging objects such as tumors hidden in turbid media (4–7). We present an analytic solution for the scattering of diffuse photon density waves (DPDWs) from spherical inhomogeneities embedded in an otherwise homogeneous medium and apply it to object imaging.

The occurrence of DPDWs has been described in detail (8, 9). In general, these waves arise when an intensity-modulated source of light is introduced into a highly scattering or diffusive medium. Microscopically, individual photons undergo a random walk within the medium. Collectively, a wave of photon density is produced that propagates spherically outward from the source. These waves have a well-defined phase and amplitude at every point in the diffusive medium. When a localized heterogeneity is embedded in the medium, the spherical wave is distorted. The degree of distortion is determined by object characteristics (such as its position, shape, size, and scattering) and absorption properties.

Since the Helmholtz equation is known to describe the transport of DPDWs in a piecewise homogeneous media (9, 10), we expect that an exact solution exists for the scattering of DPDWs by spherical objects. The solutions will be similar to, and simpler than, the theory of Mie scattering (11) often used in optics.

We derive the analytic solution of the Helmholtz equation for a piecewise homogeneous system consisting of a spherical object composed of one highly scattering medium embedded in a second highly scattering medium of infinite spatial extent. This solution is easily extended to semiinfinite media by using the extrapolated zero boundary condition (2, 12, 13). The analytic solution is compared with experimental data to assess the theory's predictive power,

and a simple inverse localization algorithm is demonstrated to determine the size and location of a spherical object. Finally, the theory is extended to include more complex problems in imaging.

THEORY

The incoherent transport of photons in a highly scattering medium is generally described by a transport equation (11, 13). In most media, however, light transport is well approximated by the diffusion equation. The approximations of the transport equation leading to the diffusion equation have been discussed (12–14). We use the diffusion approximation as the starting point of our analysis. Later we will consider errors introduced by this approximation. The time-dependent diffusion equation is

$$\nabla^2 U(\mathbf{r}, t) - \frac{\nu\mu_a}{D} U(\mathbf{r}, t) - \frac{1}{D} \frac{\partial U(\mathbf{r}, t)}{\partial t} = -\frac{1}{D} S(\mathbf{r}, t). \quad [1]$$

For diffuse light, $U(\mathbf{r}, t)$ is the photon density, ν is the speed of light in the medium, $D = \nu[3(\mu'_s + \mu_a)]^{-1}$ is the photon diffusion coefficient, μ'_s is the reduced scattering coefficient, μ_a is the absorption coefficient, and $S(\mathbf{r}, t)$ is the source term. When the intensity of a point source is sinusoidally modulated with frequency ω , U can be written as a sum of time-independent and time-dependent parts—i.e., $U = U_{DC}(\mathbf{r}) + U_{AC}(\mathbf{r})\exp(-i\omega t)$, where i is the square root of -1 (8). In this paper, we are concerned with time-dependent solutions, which, in the presence of an oscillating point source, obey the Helmholtz equation

$$(\nabla^2 + k_{AC}^2)U_{AC}(\mathbf{r}) = \frac{M}{D} \delta(\mathbf{r} - \mathbf{r}_s) \quad [2a]$$

and

$$k_{AC}^2 = \frac{-\nu\mu_a + i\omega}{D}, \quad [2b]$$

where M is the source modulation. In an infinite medium, the solution of Eq. 2a is a damped spherical outgoing wave.

In the presence of a spherical heterogeneity, $U_{AC}(\mathbf{r})$ is found by constructing a general solution to Eq. 2a outside and inside the sphere and applying the appropriate boundary conditions. It is natural to analyze the problem in spherical coordinates whose origin coincides with the center of the spherical object (Fig. 1). The general solution outside the sphere is in the form of a superposition of incident (inc) and scattered (scatt) waves (15)—i.e., $U_{out} = U_{inc} + U_{scatt}$, where

The publication costs of this article were defrayed in part by page charge payment. This article must therefore be hereby marked "advertisement" in accordance with 18 U.S.C. §1734 solely to indicate this fact.

Abbreviation: DPDW, diffuse photon density wave.

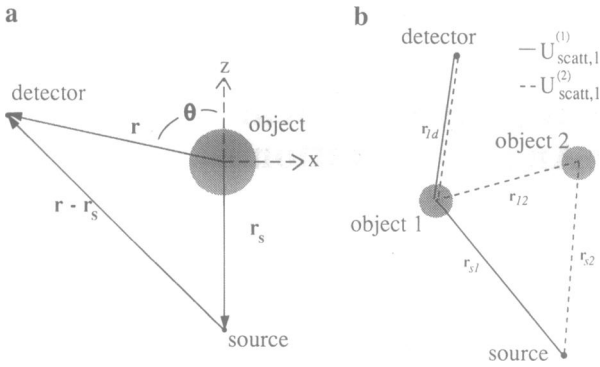


FIG. 1. To solve the Helmholtz equation for a spherical boundary, it is natural to use spherical coordinates with the origin at the center of the object (a). The source is positioned on the z axis ($\theta_s = \pi$) to exploit the azimuthal symmetry of the problem, and the relevant distances between the source, object, and detector are indicated in the figure. Scattering from multiple objects is diagrammed in b. The first- and second-order waves scattered from the first object are illustrated by solid and dashed lines, respectively. The relevant distances are indicated in the diagram.

$$U_{inc} = \frac{1}{4\pi|r - r_s|} \exp(ik^{out}|r - r_s|) = ik^{out} \sum_{l=0}^{\infty} j_l(k^{out}r_{<}) h_l^1(k^{out}r_{>}) \sum_{m=-l}^l Y_{l,m}^*(\theta_s, \phi_s) Y_{l,m}(\theta, \phi). \quad [3a]$$

and

$$U_{scatt} = \sum_{l,m} [A_{l,m} j_l(k^{out}r) + B_{l,m} n_l(k^{out}r)] Y_{l,m}(\theta, \phi). \quad [3b]$$

Inside the sphere, the general solution is

$$U_{in} = \sum_{l,m} [C_{l,m} j_l(k^{in}r) + D_{l,m} n_l(k^{in}r)] Y_{l,m}(\theta, \phi). \quad [4a]$$

Here, $j_l(x)$ and $n_l(x)$ are spherical Bessel and Neumann functions, respectively, $h_l^1(x)$ is the Hankel function of the first kind, $Y_{l,m}(\theta, \phi)$ is the spherical harmonics, k^{out} and k^{in} are the complex wave numbers outside and inside the sphere,

respectively, r (r_s) is the position of the detector (source) measured from the center of the sphere, and $r_{<}$ ($r_{>}$) is the smaller (larger) of $|r|$ and $|r_s|$. The unknown parameters ($A_{l,m}$, $B_{l,m}$, $C_{l,m}$, and $D_{l,m}$) are determined using the following boundary conditions: (i) U must be finite everywhere except at a source, (ii) U_{out} must asymptotically approach a spherically outgoing wave as $r \rightarrow \infty$, (iii) the flux normal to the boundary must be continuous; i.e., $D_{out} \nabla U_{out} = D_{in} \nabla U_{in}$, where D_{out} (D_{in}) is the photon diffusion coefficient outside (inside) the sphere, and (iv) the photon density must be continuous across the boundary; i.e., $U_{in} = U_{out}$ at $r = a$ (10, 12).

Considering these boundary conditions and using the orthogonality relation for the spherical harmonics (15), we find that for U_{out} ,

$$A_{l,m} = -ik^{out} h_l^1(k^{out}z_s) Y_{l,m}^*(\pi, 0) \times \left[\frac{D_{out} x j_l'(y) - D_{in} y j_l(x) j_l'(y)}{D_{out} x h_l^1(x) j_l'(y) - D_{in} y h_l^1(x) j_l'(y)} \right], \quad [5a]$$

and

$$B_{l,m} = iA_{l,m}, \quad [5b]$$

where $x = k^{out}a$, $y = k^{in}a$, $r_s = (r = z_s, \theta = \pi, \phi = 0)$, and j_l' and h_l^1' are the first derivatives of the functions j_l and h_l^1 with respect to the argument. Placing the source on the z axis exploits the azimuthal symmetry of the problem leading to $A_{l,m} = C_{l,m} = 0$ for $m \neq 0$. The distortion of the wave is entirely dependent on the parameters $k^{out} = k(\omega, \mu_s^{out}, \mu_a^{out})$ and $k^{in} = k(\omega, \mu_s^{in}, \mu_a^{in})$, D_{out} , D_{in} , r_s , and the object radius a . When $k^{out}a < 1$, which is true for most cases of medical interest, the infinite sum in U_{out} converges, permitting the sum to be truncated after obtaining the desired precision. The preceding calculations require no more than 20 terms in the series to obtain better than 10^{-5} precision, which far exceeds experimental precision. On a Sun Microsystems (Mountain View, CA) Sparc 2, U_{out} can be calculated 10–100 times per second (depending on the above mentioned parameters).

For the special case wherein the heterogeneity is a perfect absorber, we take the limiting form of Eq. 5 as $\mu_a^{in} \rightarrow \infty$ to determine U_{out} . Instead, one could use a more phenomenological boundary condition that requires either U_{out} to be zero

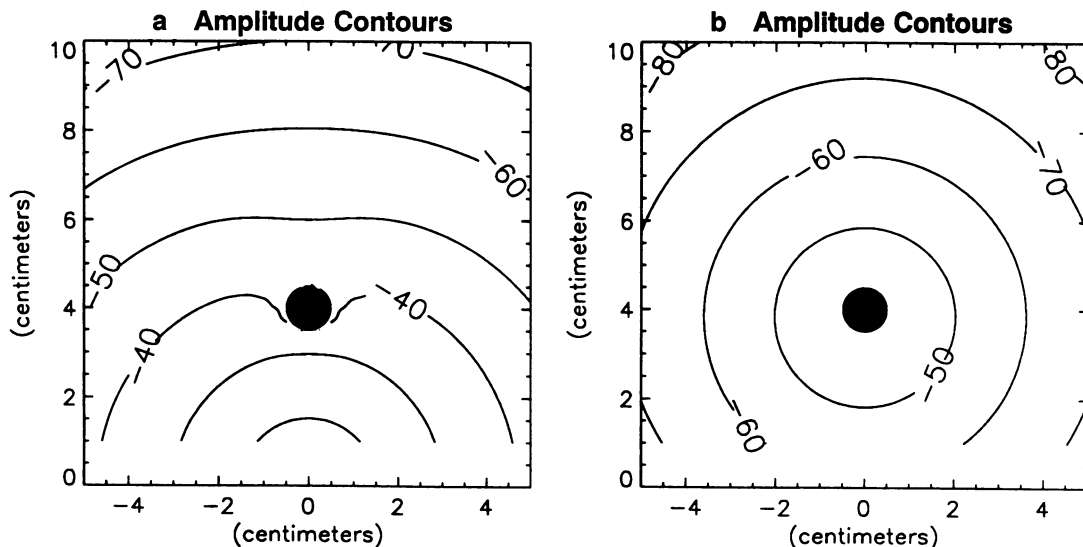


FIG. 2. Exact calculation of the wave distorted by a perfectly absorbing sphere of radius 0.5 cm positioned 4.0 cm from the source, which is at the origin, is plotted in a. The contours are of constant amplitude and are plotted in intervals of 10 decibels (dB). For these plots, the surrounding medium's optical characteristics are $\mu_s' = 10 \text{ cm}^{-1}$ and $\mu_a = 0.02 \text{ cm}^{-1}$, the modulation frequency is 200 MHz, and $v = 2.25 \times 10^{10} \text{ cm/s}$. The amplitude of the scattered wave is plotted in b, where the contours are drawn every 10 dB.

on an extrapolated boundary (2, 12, 13) or the outward radial component of the flux to be zero on the boundary; however, we found that the resulting differences were small.

The photon density outside the sphere is a superposition of the incident wave and a scattered wave. Constant amplitude contours of U_{out} and U_{scatt} in the presence of a perfect absorber are plotted in Fig. 2. The distortion of the wave front will decrease with absorber size because, to leading order, the intensity of the scattered wave is proportional to ka [i.e., the $A_{l,m} \approx (ka)^{2l+1}$]. It is interesting to note that the scattered wave becomes more isotropic for smaller objects. Analytically this arises because as ka decreases the contribution from the higher order ($l > 0$), partial waves become less significant compared to the $l = 0$ spherical partial wave. These results are consistent with recent "difference" measurements performed on absorbing spheres by Sevick *et al.* (16).

The analytic solutions enable us to estimate the measurement precision required to detect ideal objects. The required phase precision is determined from the position-dependent difference in phase between the incident wave and the distorted wave, while the required amplitude precision is found from the position-dependent ratio of $|U_{out}|/|U_{inc}|$. Contour plots of the phase difference and the amplitude ratio indicate the spatial positions that are most sensitive to the presence of the object as well as the required signal-to-noise ratio. Fig. 3 illustrates this spatially dependent sensitivity for a perfectly absorbing sphere immersed in a medium with $\mu'_s = 10.0 \text{ cm}^{-1}$ and $\mu_a = 0.02 \text{ cm}^{-1}$. These plots show that 1.0° phase and 10.0% amplitude precision is sufficient for localization with measurements made in the shadow (within 4.0

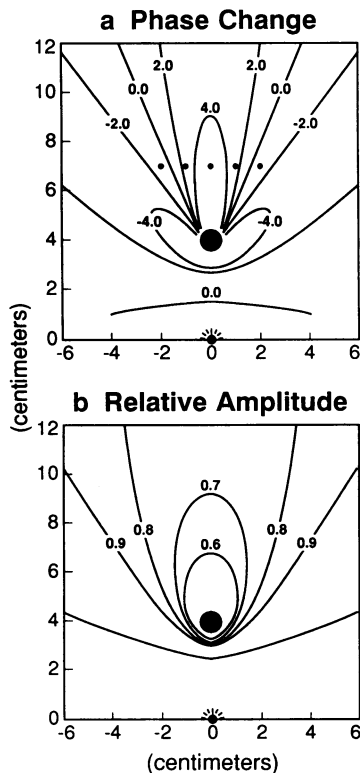


FIG. 3. These sensitivity plots demonstrate the phase and amplitude resolution necessary to measure a DPDW distorted by a perfect absorber. (a) Phase difference between an incident wave and the wave distorted by a 1.0-cm-diameter absorber. (b) The ratio of the amplitude of the distorted wave with respect to the incident wave. For these plots, the surrounding medium's optical characteristics are $\mu'_s = 10 \text{ cm}^{-1}$ and $\mu_a = 0.02 \text{ cm}^{-1}$, the modulation frequency is 200 MHz and $v = 2.25 \times 10^{10} \text{ cm/s}$. The dots in *a* represent the locations where measurements were made to characterize the object.

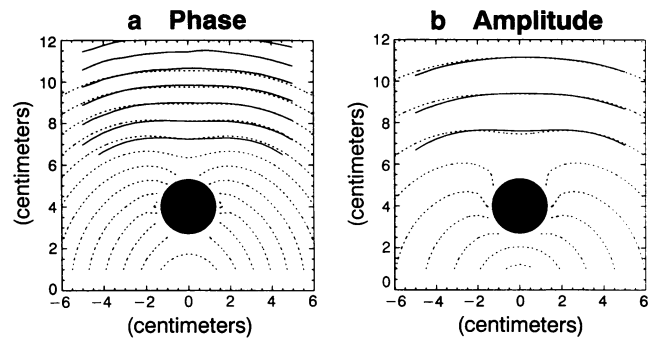


FIG. 4. Experimental measurements (solid lines) of a DPDW distorted by a 1.3-cm-radius perfect absorber are compared to the theoretical prediction (dotted lines) for the given experimental parameters. Phase contours are drawn every 20° in *a*, and the amplitude contours are drawn every 10 dB. For this experiment, the optical properties of the surrounding medium were $\mu'_s = 3.0 \text{ cm}^{-1}$ and $\mu_a = 0.02 \text{ cm}^{-1}$, $\omega = 200 \text{ MHz}$, and $v = 2.25 \times 10^{10} \text{ cm/s}$.

cm of the object) of the 1.0-cm-diameter absorber. This is well within the 0.1° phase and 0.1% amplitude precision available with current detectors. Localization of smaller absorbers will require better precision.

EXPERIMENTAL DESIGN

The experimental setup has been discussed in detail (9) and is briefly described here. We modulate a 780-nm output of a 5-mW laser diode at 200 MHz. Photons from the source are guided through a 6.0-mm-diameter fiber optic cable into a 60-liter tank containing a turbid medium called Intralipid.[§] The scattering medium is essentially infinite and is homogeneous except for the small spherical inhomogeneity, a black sphere, that is suspended in a fixed position from the top of the tank. Measurements of the relative photon density (17) are made by positioning one end of a detection fiber in the Intralipid at a known location relative to the source and attaching the other end to a photomultiplier tube. The signal is heterodyned down to 25 KHz and is analyzed by lock-in techniques to obtain the phase and amplitude of the photon density. The wave is detected in this way as a function of position within the tank.

Two sets of experiments were performed, one to check the validity of the theory and the other to resolve object characteristics by fitting the theory to experimental data. The optical properties of the given concentration of Intralipid were determined before each experiment through separate measurements of phase and amplitude of the DPDW propagating in the infinite homogeneous system (3, 8). These quantities were used in our subsequent analysis.

In the first set of experiments, the object and source are fixed in the Intralipid with a separation z_s . The phase and amplitude of the distorted DPDW are measured by moving the detector to different points on a two-dimensional grid containing the source and the center of the object. These experimental results are then compared to the prediction of Eq. 3 for the given object properties.

In the second set of experiments, the properties of different spherical absorbers are found by fitting the theory to a measurement of the distorted wavefront along a line. This was accomplished by minimizing the least squares theoretical fit to the experimental data with respect to object position relative to the source and object radius.

[§]Intralipid is a polydisperse suspension of fat particles ranging in diameter from $0.1 \mu\text{m}$ to $1.1 \mu\text{m}$. The Intralipid used here was obtained from the hospital of the University of Pennsylvania.

Table 1. Results of fitting theory to a series of experimental observations of a DPDW scattered by an absorber

Exp.	Z_{detector} , cm	Intralipid, %	l^* , cm	Z_{fit} , cm	X_{fit} , cm	Y_{fit} , cm	a_{fit} , cm
A	6.5	0.25	0.60	3.87	-0.05	0.08	1.02
B	7.5	0.25	0.60	4.08	-0.06	-0.56	1.04
C	6.5	0.50	0.33	4.06	0.00	-0.13	1.12
D	7.5	0.50	0.33	4.01	-0.02	0.08	1.15
E	6.5	0.75	0.23	4.20	0.01	-0.07	1.15
F	7.5	0.75	0.23	4.11	0.00	0.12	1.20
G	6.5	1.00	0.18	4.12	0.02	0.00	1.22
H	7.5	1.00	0.18	4.17	0.00	0.04	1.21

Absorber had a radius of $a_{\text{exp}} = 1.3$ cm and was positioned at $Z = 4.0$ cm, $X = 0.0$ cm, and $Y = 0.0$ cm. For each experiment, the detector was positioned at Z_{detector} and scanned from -2.0 cm $< X < 2.0$. The experiments were performed in different concentrations of Intralipid for which the photon random walk step is given by l^* , where $l^* = 1/\mu'_s$. In all experiments, $\mu_a = 0.02$ cm $^{-1}$, $\omega = 200$ MHz, and $v = 2.25 \times 10^{10}$ cm/s.

RESULTS

Our measurements indicate that the analytic theory accurately predicts the distortion of the DPDW. Furthermore, because of the close agreement, we are able to characterize a spherical absorber embedded in the turbid medium. These observations were not obvious *a priori* for one major reason: our theory is derived from the diffusion equation, but photon migration is better approximated by a transport equation. In fact, significant differences between the diffusion equation and the transport equation arise near sharp boundaries. As mentioned below, we have detected evidence of these differences.

The measured distortion of the DPDW by a perfectly absorbing sphere is shown in Fig. 4 and compared to the predicted distortion. This comparison illustrates that the analytic solution shows good agreement with the experimental data.

As an example of the utility of the analytic solution, we have compared theory to measurements of phase and amplitude of the DPDW along lines parallel to those indicated in Fig. 3a to predict object size and location. The results of these experiments are presented in Table 1. Fits for two of these experiments are shown in Fig. 5.

The results in Table 1 show that a fit to measurements made in the shadow of the object determines the x and y position of the absorber to an accuracy of ± 0.1 cm and the z position to ± 0.2 cm. Finally, the object radius was determined to within ± 0.3 cm. With a decrease in the photon random walk step, the discrepancy between the determined radius and the known radius is seen to decrease. This trend is a result of applying the diffusion equation to a system with a sharp absorbing boundary.

APPLICATIONS

In this section, we demonstrate the extension of the analytic solution toward other imaging scenarios.

Phased Sources. Measurements made with a phased source are highly sensitive to the presence of heterogeneities (6, 18). A simple phased source consists of two oscillating light sources of equal amplitude that are 180° out of phase and are separated by a small distance. In a homogeneous medium, the DPDWs generated by each source interfere to create a nodal plane of zero amplitude across which the phase shifts by 180° . The presence of an inhomogeneity distorts this nodal plane into a quasinodal surface.[¶] Inhomogeneities may be detected by measuring the distortion of the quasinodal surface.

In the presence of a spherical object, the position-dependent photon density generated by a system of sources

is easily calculated by summing Eq. 3 for each source. This solution is useful in analyzing the effectiveness of using phased sources to characterize hidden objects in comparison to single sources.

Scattering from Multiple Objects. Another important scenario involves samples that contain two or more spherical objects. In this case, the distorted wave is calculated by summing scattering events of different order. We first calculate the scattering of the incident wave from each object. This is the first-order scattered wave. The first-order scattered waves are incident on and, consequently, scattered by the surrounding objects resulting in second-order scattered waves whose amplitude is smaller than the first-order wave. For two spherical objects embedded in an infinite homogeneous medium, the general solution is of the form

$$U_{\text{out}} = U_{\text{inc}} + \sum_{n=1}^{\infty} (U_{\text{scatt},1}^n + U_{\text{scatt},2}^n), \quad [6]$$

where $U_{\text{scatt},i}^n$ is the n th-order scattered wave from the i th object (see Fig. 1). While the first-order waves ($U_{\text{scatt},i}^1$) are easily calculated using Eq. 3, the second-order waves ($U_{\text{scatt},i}^2$) require the solution of complex integral equations. The dominant portion of $U_{\text{scatt},i}^2$, however, can be computed analytically; it is the $l = 0$ component of $U_{\text{scatt},j}^1$ scattering from the i th object ($i \neq j$). The significance of the second-order wave can be estimated by the ratio of $U_{\text{scatt},i}^2$ to U_{inc} . Our comparisons find that $U_{\text{scatt},i}^2$ is negligible in most cases.^{||} The distortion of a DPDW by several objects is thus accurately computed using only the first-order scattered waves.

Semifinite Media. In medical imaging, measurements are typically made by placing the source and detector on the skull or breast tissue. Treating such a system as infinite is obviously incorrect and will lead to discrepancies between theory and experiment. Planar boundaries between diffusive and nondiffusive media can be modeled by requiring $U_{\text{out}} = 0$ on an extrapolated zero boundary a distance $z_0 = 0.7104/\mu'_s$ from the actual boundary, away from the diffusive medium (2, 12, 13). Multiple planar boundaries can be modeled by employing additional zero boundary conditions. To first order, the zero amplitude boundary condition is satisfied by placing an image source of negative amplitude at the position of the actual source reflected about the zero boundary. The photon density is then calculated by superimposing the DPDWs generated by the two sources and their respective scattered waves. In general, one must also consider an image of the scattered waves to ensure that U_{out} equals zero on the extrapolated

[¶]In the presence of an inhomogeneity, the nodal plane is perturbed into a surface across which there is a large change in phase (of order 180°) and on which the amplitude is a minimum rather than zero. We refer to this new surface as a quasinodal surface.

^{||}Second-order scattered waves are negligible when $(r_{sd}a^2)/(r_{si}r_{jd}) |\exp[ik(r_{si} + r_{ij} + r_{jd} - r_{sd})]| \ll 1$ where i and j denote the different objects (see Fig. 1).

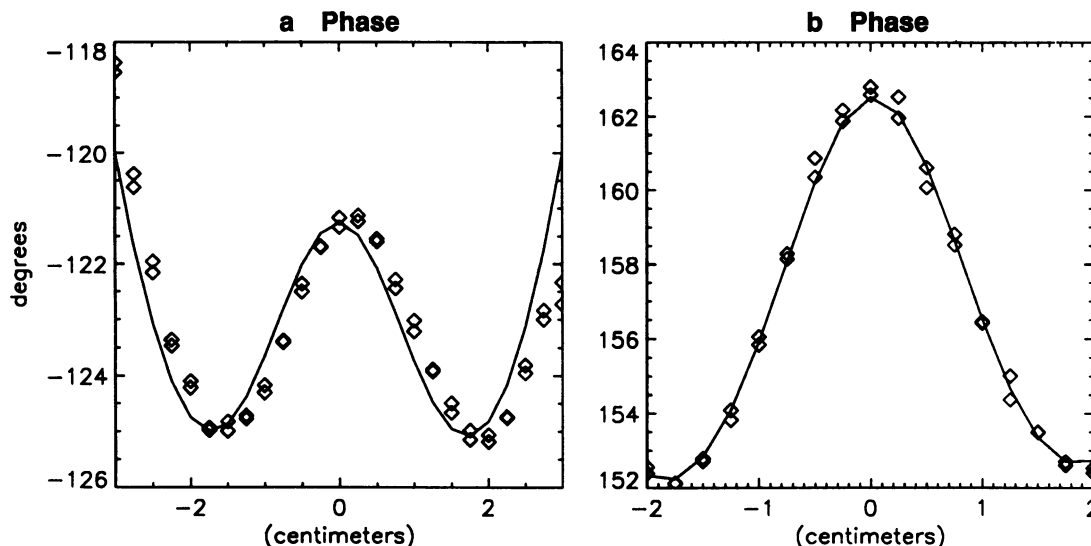


FIG. 5. Fits to experiments C and G from Table 1 are presented in *a* and *b*, respectively. The experimental data (\diamond) are compared to the best fit (solid line). The experimental parameters are given in Table 1.

zero boundary. These images then create waves that scatter off the object, *ad infinitum*.

Comparing calculations for semiinfinite and slab systems with infinite systems, we found that the wavefronts have the same general shape except near the boundaries and that the object sensitivity is unaffected by the boundaries.

Time-Domain Measurements. Our scattering theory is easily extended to the time domain. A pulse of light propagating in a turbid medium can be thought of as a superposition of many DPDWs with different modulation frequencies. Thus, a time-resolved measurement of the propagation of a light pulse is an easy way to determine the frequency response of the system (19). To calculate the response to a pulse of light, we simply compute the scattering due to each DPDW in parallel.

We computed the temporal evolution of a light pulse with width $\tau = 10$ ps and period $T = 1.0$ μ s in an infinite medium with different-sized perfect absorbers. The results indicate that the measured photon density will decrease as a result of an absorber but that the decay rate of the light energy density is relatively unaffected by its presence. These results are consistent with the experimental observations of Liu *et al.* (20).

CONCLUSIONS

We have presented an analytic solution of the Helmholtz equation for the scattering of diffuse photon density waves from spherical objects embedded in an otherwise homogeneous turbid medium. Our experimental observations demonstrate that this solution can be used in conjunction with a simple imaging algorithm to characterize spherical objects. Finally, the analytic solution permits a straight forward approach to the complicated analysis of measurements made with phased sources, scattering from multiple objects, the effect of planar boundaries, and measurements made in the time domain. We will present these latter results in greater detail elsewhere.

It is a pleasure to acknowledge useful conversations with Hanli Liu, Andreas Hielscher, Peter Kaplan, Michael Cohen, and Kyung Kang. A.G.Y. gratefully acknowledges partial support from the National Science Foundation through the Presidential Young Inves-

tigator Program and Grant DMR-9003687 and from the Alfred P. Sloan Foundation. This work was also supported by National Institutes of Health Grants NS-27346, HL-44125, and CA-50766/60182.

1. Chance, B. (1989) *Photon Migration in Tissues* (Plenum, New York).
2. Patterson, M. S., Chance, B. & Wilson, B. C. (1989) *Applied Optics* **28**, 2331–2336.
3. Tromberg, B. J., Svaasand, L. O., Tsay, T. & Haskell, R. C. (1993) *Applied Optics* **32**, 607–616.
4. Chance, B., ed. (1991) *Future Trends in Biomedical Applications of Lasers*, SPIE Proceedings (SPIE, Bellingham, WA), Vol. 1525.
5. Maier, J. & Gratton, E. (1993) *Proc. SPIE Int. Soc. Opt. Eng.* **1888**, 440–451.
6. Knuttel, A., Schmitt, J. M. & Knutson, J. R. (1993) *Applied Optics* **32**, 381–389.
7. Boas, D. A., O’Leary, M. A., Chance, B. & Yodh, A. G. (1993) *Phys. Rev. E* **47**, R2999–R3002.
8. Fishkin, J. B. & Gratton, E. (1993) *J. Opt. Soc. Am. A* **10**, 127–140.
9. O’Leary, M. A., Boas, D. A., Chance, B. & Yodh, A. G. (1992) *Phys. Rev. Lett.* **69**, 2658–2661.
10. Carslaw, H. S. & Jaeger, J. C. (1959) *Conduction of Heat in Solids* (Oxford Univ. Press, Oxford).
11. Ishimaru, A. (1978) *Wave Propagation and Scattering in Random Media* (Academic, New York), Vol. 1.
12. Glasstone, S. & Edlund, M. C. (1952) *The Elements of Nuclear Reactor Theory* (Nostrand, New York), Chapt. 5 and 14.
13. Case, K. M. & Zweifel, P. F. (1967) *Linear Transport Theory* (Addison-Wesley, Reading, MA), Chapt. 8.
14. Fishkin, J., Gratton, E., van de Ven, M. J. & Mantulin, W. M. (1991) *Proceedings of Time-Resolved Spectroscopy and Imaging of Tissues* (SPIE, Bellingham, WA).
15. Jackson, J. D. (1975) *Classical Electrodynamics* (Wiley, New York), Chapt. 3 and 16.
16. Sevick, E. M., Lakowicz, J. R., Szmajkowski, H., Nowaczyk, K. & Johnson, M. L. (1992) *J. Photochem. Photobiol. B* **16**, 169–185.
17. Liu, F., Yoo, K. M. & Alfano, R. R. (1993) *Optics Lett.* **18**, 432–434.
18. Chance, B., Kang, K., He, L., Weng, J. & Sevick, E. (1993) *Proc. Natl. Acad. Sci. USA* **90**, 3423–3427.
19. Kang, K. A., Chance, B., Bruley, D. F. & Londono, J. M. (1993) *Proc. SPIE Int. Soc. Opt. Eng.* **1888**, 340–353.
20. Liu, H., Miwa, M., Beauvoit, B., Wang, N. G. & Chance, B. (1993) *Anal. Biochem.* **213**, 378–385.